Hindawi
Journal of Nanomaterials
Volume 2022, Article ID 2460364, 9 pages
https://doi.org/10.1155/2022/2460364

Research Article

Nanocomposites of GO/D-Mannitol Assisted Thermoelectric Power Generator for Transient Waste Heat Recovery

Lourdu Jame,[1] **Suresh Perumal**,[2] **Manojkumar Moorthy**,[2] **and Joselin Retna Kumar**[3]

[1]*Department of Electrical and Electronics Engineering, SRM Institute of Science and Technology, Kattankulathur, Chengalpattu, 603203 Tamilnadu, India*
[2]*Laboratory of Energy and Advanced Devices (LEAD), Department of Physics and Nanotechnology, SRM Institute of Science and Technology, Kattankulathur, Chengalpattu, 603203 Tamilnadu, India*
[3]*Department of Electronics and Instrumentation Engineering, SRM Institute of Science and Technology, Kattankulathur, Chengalpattu, 603203 Tamilnadu, India*

Correspondence should be addressed to Joselin Retna Kumar; joselinr@srmist.edu.in

Received 7 October 2021; Revised 26 December 2021; Accepted 28 March 2022; Published 14 April 2022

Academic Editor: Ana Espinosa

Thermoelectric generators (TEGs) have received a great attention in the field of renewable energy resources due to their superior ability of converting untapped waste heat into usable electricity. In order to boost the conversion efficiency of TEG and to retrieve the transient heat, this paper demonstrates the role of nanostructured graphite (G) and graphene oxide (GO) decorated phase-change material (PCM) of D-mannitol attached with the hot end of commercial thermoelectric module on enhancement of conversion efficiency and power output. Presence of G and GO on the matric of D-mannitol has been confirmed by powder XRD and FE-SEM. The open circuit voltage (V_{oc}) and short circuit current (I_{sc}) of TEG attached with PDM, G/PDM, and GO/PDM were recorded for the heating and cooling cycles in the temperature range of 325-450 K. Particularly, the experimentally measured V_{oc} and I_{sc} of TEG with only PDM are 1.23 V and 90 mA, respectively, for the temperature difference of $\Delta T \backsim 118$ K, whereas the maximum V_{oc} of TEG attached with GO/PDM drawn in presence of an external heater is 4.5 V for $\Delta T \backsim 118$ K. Further, the maximum output power of TEG with GO-PCM drawn in the heater-ON and heater-OFF is 1012.5 mW and 450 mW, respectively.

1. Introduction

Excessive consumption of fossil fuels and energy demand for mankind led to severe ecological difficulties, such as climate change, ozone layer depletion, and global warming [1]. Waste heat recovery can be one of the important solutions to recover waste heat that is released from the automobile exhausts, power plants, and metallurgical industries which could be converted into usable electricity using thermoelectric (TE) materials. Generally TE generators (TEGs) work on the principle of Seebeck effect where one end of the TEG kept at hot side and other end is maintained at low temperature that generates voltage across the TEG. A TE module has large number of *p*-type and *n*-type thermoelements connected electrically in series and thermally in parallel [2–5].

The efficiency of TEG can be defined through a relation [3]

$$\eta = \frac{T_{hot} - T_{cold}}{T_{hot}} \left(\frac{\sqrt{1 + z\bar{T}} - 1}{\sqrt{1 + z\bar{T}} + T_{cold}/T_{hot}} \right), \quad (1)$$

where T_{hot} and T_{cold} are temperatures of hot-end and cold-end temperature of TEGs, respectively. Further, $z\bar{T}$ is the figure-of-merit which can be defined through a relation given below.

$$zT = \frac{S^2 \sigma T}{\kappa_{\text{total}}}, \quad (2)$$

where S, σ, κ_{total}, and T stand for Seebeck coefficient, electrical conductivity, total thermal conductivity, and temperature, respectively.

Typically, TE modules are classified based on the operating temperature such as low temperature (300-525 K), medium (500-900 K), and high temperature (900 K) TEGs with appropriate p and n-type materials of Bi_2Te_3, PbTe, and SiGe, respectively [2–8]. Based on the operating temperatures, TEGs can be used in various applications such as biomedical applications, microsensors, power generation from automobiles, and space [6–9]. However, the main barriers for the development of TEG are (i) relatively less efficiency, (ii) issues on contact materials, (iii) parasitic losses on the TE devices, and (iv) constant maintenance of temperature difference [2, 3].

Nevertheless, commercially available TEGs are mostly based on Bi_2Te_3 materials, which are salient to recover the waste heat when temperature difference is constantly maintained. Most of the heat releasing resources, such as car exhausts, heat plants, and metallurgical laboratories, are transient in nature which has to be stored and employed effectively. In this content, phase-change materials (PCMs) are known for their superior heat storage [10] and release of latent heat which made them to use it in solar-based space power generation, industrial waste heat recovery, textiles, buildings, air conditioning systems, and electronic cooling [11–13]. However, low heat transfer rate of PCM can be improved by adding high thermal conductivity material with PCM [14]. Additionally, thermal conductivity of PCM can also be further enhanced by forming fin structure, capsule structure, and porous medium structures [15–17]. For powering sensors in aircraft wings, thermoelectric generators (TEGs) with phase-change material are effectively used [18, 19]. To enhance reverse power generation, experimental investigation of cupric acid PCM integrated with TEG was done and obtained V_{oc} of 3.3 V for the heat flux of 2250 W/m^2 which can be an efficient method of cooling the electronic devices [20]. Saeed et al. have investigated two-stage thermoelectric power generation (TTEG) system with phase-change materials which generates the conversion efficiency of 27% more potential than the single-stage TEG, and it is most suitable for wireless sensor nodes (WSNs). TTEG produces the open circuit voltage of 0.38 V for the time duration of 7900 sec when heater is off, while the single-stage TEG generates the same voltage within the time period of 2100 sec [21]. Additionally, different position (hot side, cold side, and both side) of aluminum box filled with PCM is compared with normal TEG without PCM, whereas PCM in the hot side can protect the TE device from high temperature [22]. Different nanofillers such as carbon fiber, graphene nanoplatelets, and multiwalled carbon nanotubes with paraffin-based PCM were compared, and it is observed that the improvement was obtained using graphene nanoplatelets [23]. Moreover, the integration of multiwalled CNTs and Al_2O_3 nanoparticle with paraffin PCM reduces the thermal resistance and slightly increases the phase-change temperature [24]. Manikandan et al. [25] have examined the performance of low concentrated photovoltaic module (CPV) with phase-change material by varying heat input, fin quantity, solar concentration ratio, and amount of PCM. The CPV temperature was maintained constant during the phase change of the PCM which indeed increased the power output and efficiency of CPV to 22% and 27% higher than the case without PCM. Jame et al. [26] have investigated the performance of D-mannitol PCM kept in the hot side of TEG to recover transient heat to boost the conversion efficiency. It generates an open circuit voltage of 1.23 V, and in the presence of heater-on and heater-off condition, the maximum power drawn is 20.8 mW and 0.48 mW. In reference [27], due to aerodynamic heating in flights, more amount of heat is wasted. In order to improve the structural heat conduction, PCM along with TEG is used and this composite structure reduces maximum temperature by 180 K and maximum thermal stress by 110 Mpa. Output power improved by 64.8% through structural optimization under flight condition.

Here, we demonstrate and validate the transient heat storage and power generation performance of TEG with nanoenhanced D-mannitol PDM. A special experimental setup was designed and examined to recover the transient waste heat and convert them into a useful electrical energy. An aluminum container filled with G/PDM and GO/PDM kept in between the external heater and the hot end of TEG. During heater-on condition, heat is absorbed by PDM and the maximum open circuit voltage obtained with G/PDM and GO/PDM was 2.5 V and 4.5 V where cold-side temperature is maintained at 301 K. In closed circuit condition, due to drop across internal resistance, the maximum voltage of G/PDM and GO/PDM thus obtained reduces to 1.25 V and 2.25 V. Interestingly, at heater-off condition, G/PDM and GO/PDM release the stored heat energy from PCM to TEG which produces the maximum power of 23 mW and 73 mW. Particularly, at heater-off condition, the generated voltage persists for 40 minutes which suggests that in the absence of external thermal energy, the transient heat can be effectively stored via G- and GO-embedded PCM material that could be performed as hot-side temperature of TEG and thereby TEG can continuously generate the power.

2. Experimental Section

2.1. Preparation of Graphene Oxide. With a concern to synthesis, the graphene oxide using Hummer's method, graphite flakes (2.5 g), and sodium nitrate (2.5 g) were added in a 1000 ml beaker with 50 ml of concentrated sulphuric acid (H_2SO_4). The reaction mixture should be stirred for 2 hours in an ice bath (0-5°C), where potassium permanganate ($KMnO_4$) (8 g) was added to the reaction mixture and maintain a reaction temperature lower than 288 K. The ice bath was removed later, and the reaction mixture continuously stirred at 308 K until it forms colloidal solution. The reaction mixture at a temperature of 371 K was diluted with 120 ml deionized water with effervescence, and a color changes to brown was observed. Finally, the solution is treated with 15 ml of H_2O_2 (30%) to terminate the reaction by removing -COOH group and excess oxides. Here, color of solution turns into yellow. The resulting mixture was washed with DI water and 10% diluted HCl and centrifuged at 5000 rpm to remove unwanted residues [28].

2.2. Preparation of PCM Material. High pure (~99.99%) phase-change material (PDM) of D-mannitol was procured from Alfa Aesar. Powder of PDM (30 g) was taken in a beaker and heated at 453 K for 2 hours so as to reach its phase-change temperature. The melted PDM was stirred at 1000 rpm for 1 hour to have high homogeneity of PCM, and then, melted PCM was transferred into an aluminum container, and the sample is labelled as PDM. For making G/PDM (PCM with graphite powder), the melted D-mannitol (30 g) was mixed with graphite powder (0.3 g) and stirred at the rotation speed of 1000 rpm for 2 hours to have high homogeneity of G/PDM and sealed in an aluminum container without any leakages. For making GO/PDM (PCM with nanostructured graphene oxide), melted D-mannitol (30 g) mixed with graphene oxide (0.3 g) is taken in a beaker, and to have high homogeneity, it is stirred at the rotation speed of 1000 rpm for 2 hours. The final sample from the magnetic stirrer was poured in an aluminum PCM container and properly sealed without any leakages.

2.3. Design and Fabrication of TE Efficiency Measurement System. Thermoelectric (TE) efficiency measurement system was designed and fabricated indigenously, as shown in Figure 1. The input heat to the hot side of TEG is supplied by the electric heater. Ceramic wafer insulated TE module is kept in between copper plates and mica sheets for uniform heat distribution. In order to improve the heat transfer, thermal grease is pasted on the hot and cold side of TEG. In the cold side of TE module, water is circulated by the submersible pump and a chiller is used to cool the cycled water. Three mechanical springs are used in the TE efficiency measurement system to ensure proper thermal contact across cold and hot side of TEG. To measure the load voltage (V_L) and load current (I_L) under closed circuit condition, the load resistance of 4.5 Ω was connected in output leads of the TEG.

According to the dimension of TE device, an aluminum container was designed with a dimension of 40 mm × 40 mm × 100 mm where the melted samples of only PCM, G/PCM, and GO/PCM were filled inside and sealed without any leakages. Figure 2 shows the block diagram representation of PCM attached TEG in the TE efficiency measurement system. For measuring hot side and cold-side temperature, two thermocouples were connected at the bottom and top of TEG. The uncertainty of experimental setup is typically less than 5%. Multimeter (MS8040) was used to measure open circuit voltage (V_{OC}), load voltage (V_L), and load current (I_L).

2.4. Characterization Techniques

2.4.1. X-Ray Diffraction (XRD). Powder X-ray diffraction is performed on PDM, G/PDM, and GO/PDM using BRUKER D8 Advance, with Cu-Kα radiation (λ = 1.5406 Å) to identify its phase purity and presence of graphite and graphene oxide in the matrix of D-mannitol. The Bragg's diffracted angle 2Θ was recorded from 10 to 100 degrees with a step size of 0.03.

2.4.2. Scanning Electron Microscope (SEM). Powders of PDM, G/PDM, and GO/PDM were analysed using high-resolution scanning electron microscope (HR-SEM) (Thermo Scientific Apreo S, USA) to investigate the surface morphology and elemental composition.

2.4.3. Differential Scanning Calorimetry (DSC). Phase and thermal stability analysis was performed on PDM, G/PDM, and GO/PDM using differential scanning calorimetry (DSC STA2500, NETZSCH, Germany). The analysis was performed using 2.9 mg of PDM, under N_2 atmosphere at a flow rate of 40-60 ml/min. For all the samples, pierced aluminum (Al) was used as reference.

3. Results and Discussions

3.1. Powder X-Ray Diffraction. Figure 3 presents the powder X-ray diffraction pattern of PDM, G/PDM, and GO/PDM. PDM thus commercially purchased from Alfa Aesar adopts the orthorhombic structure with a space group of $P2_12_12_1$ which could be indexed with the (JCPDS 00-008-0753). Further, samples of graphite (G) and graphene oxide (GO) have also taken for PXRD and Bragg's peak at 2Θ of 11 with corresponding plane of 002 confirms the graphite whereas graphite oxide (GO) was confirmed by the plane of 001 at the Bragg's peak of 26. Presence of G and GO on the matrix of PDM was also confirmed from the powder XRD pattern. The lattice parameters for PDM powder were calculated from using unit cell software, and it is found to be a = 8.694 Å, b = 16.791 Å, and c = 5.543 Å with a unit cell volume (V_{cell}) = 809 Å^3.

3.2. Scanning Electron Microscope Micrograph. Figure 4 presents the scanning electron micrographs of PDM, G/PDM, and GO/PDM powders. The powder morphology of PDM shows a random morphology with mixed agglomerated structures, as shown in Figure 4(a). Presence of graphite and graphene oxide in the matrix of PDM is seen as layered sheets, as illustrated in Figures 4(a) and 4(b). The GO/PDM is also evidently convinced to have layered sheet structures and corresponding EDX spectra confirms the presence of carbon and oxygen in equiatomic ratio.

3.3. Differential Scanning Calorimetry (DSC) Analysis. DSC curves of PDM, G/PDM, and GO/PDM show the melting and crystallizing processes in temperature range of 350-455 K. Figure 5 clearly distinguishes the phase transition of PDM, G/PDM, and GO/PDM, and the heating rate was maintained as 5°C per minute in the measured temperature range. From Figure 5, the PDM sample is entirely in solid phase from room temperature to 433 K, after which an endothermic sharp peak starts at a temperature of 436.8 K and reaches its maximum at 440.1 K, where complete melting is observed. On the other hand, sample of G/PDM shows the slightly different trend where the melting starts at 435 K and reaches its maximum at 442 K. Moreover, in GO/PDM sample, the melting starts at 435 K, and peak melting is observed at 437 K. Further, it is inferred that the strong C-C bond in graphite has contributed to higher melting temperature as the bond breaking requires higher energy than GO and pure samples. The uncertainty of DSC measurement is typically less than 5%.

3.4. Open Circuit Voltage of TEG. Figure 6(a) shows open circuit voltage (V_{OC}) with respect to time for only PDM, G/PDM, and GO/PDM. From the graph, it is clearly understood

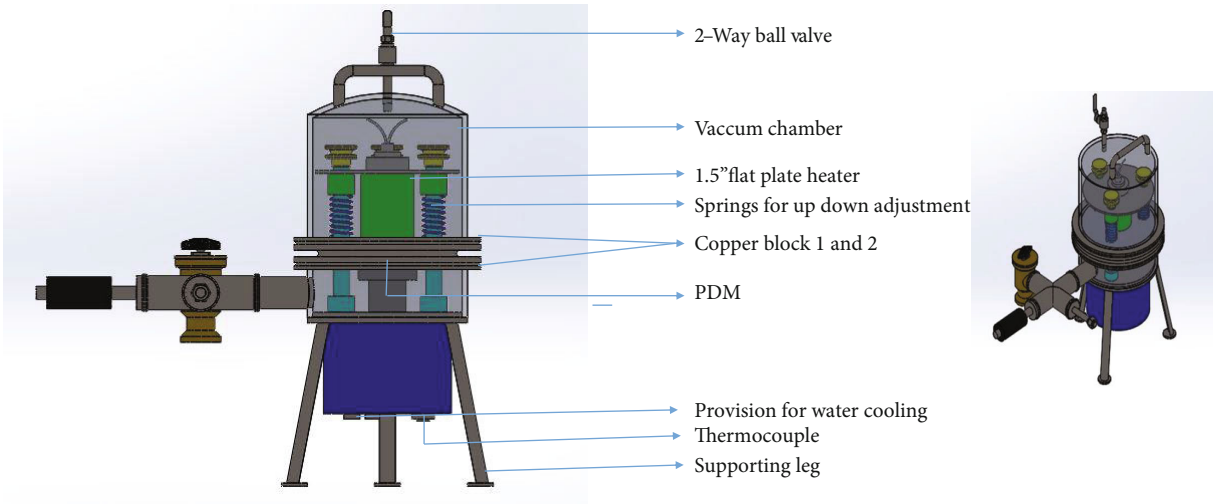

Figure 1: Top view and front view of thermoelectric efficiency measurement system.

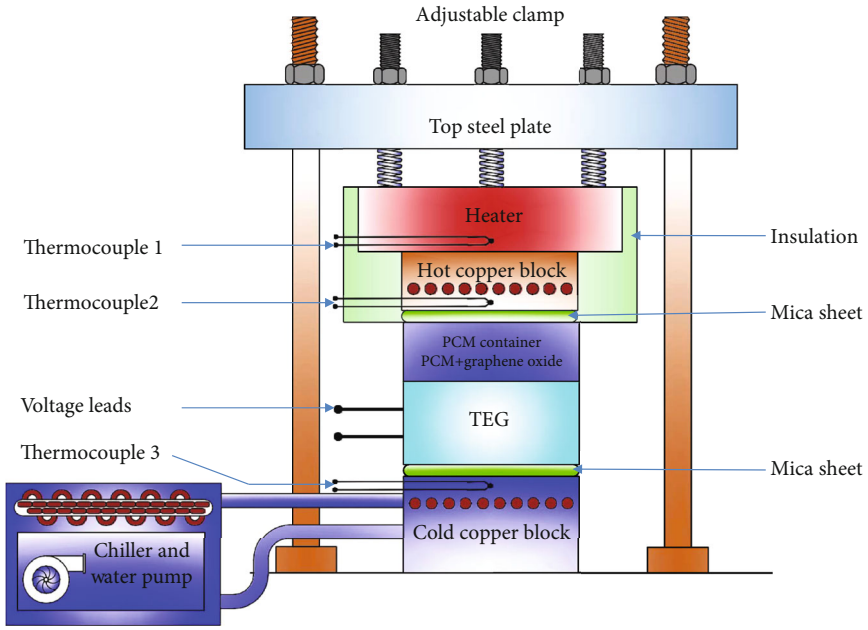

Figure 2: Schematic diagram of PCM attached TE efficiency measurement system.

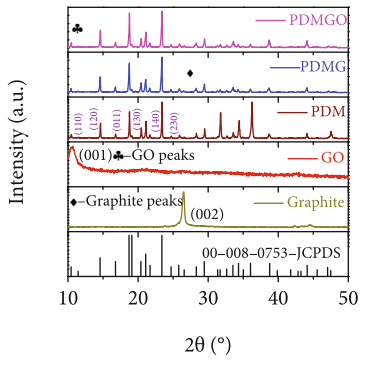

Figure 3: Powder XRD pattern of PDM, G/PDM, and GO/PDM samples.

that the melting of PDM takes place after 90 minutes and reaches the peak melting point at 150 minutes. When nanomaterials such as GO, G added with PDM, thermal conductivity of PDM is increased, and improved heat transfer is obtained whereas melting of G/PDM starts at 30 minutes and reaches sharp melting point at 65 minutes. Due to the improved thermal conductivity of GO/PDM, melting starts immediately after 10 minutes and reaches peak melting point at 30 minutes.

Figure 6(b) shows the open circuit voltage with respect to hot side of TEG. During open circuit condition, an external heater is used to supply heat to PDM which gradually rises the temperature of TEG at hot side, where cold side is maintained at 301 K. Due to the temperature difference across the hot and cold side of TEG, there is a voltage

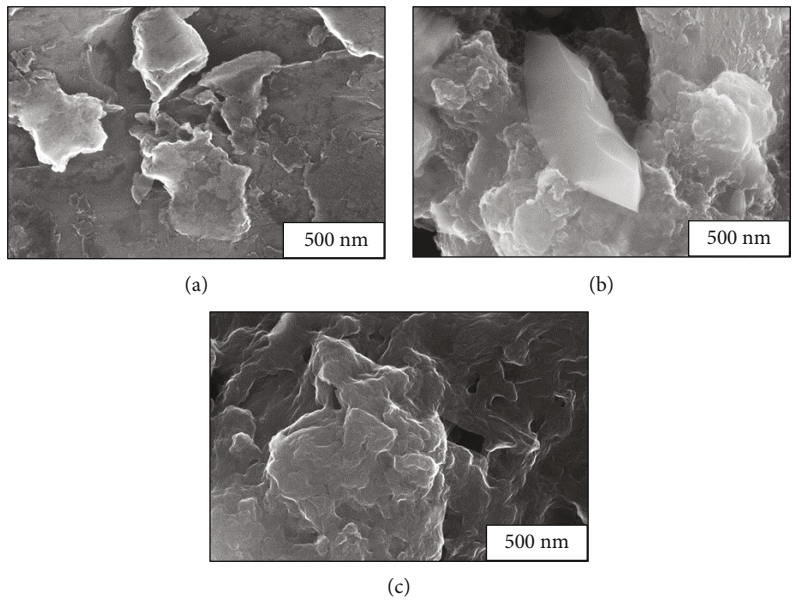

Figure 4: FE-SEM micrographs of (a) PDM, (b) G/PDM, and (c) GO/PDM.

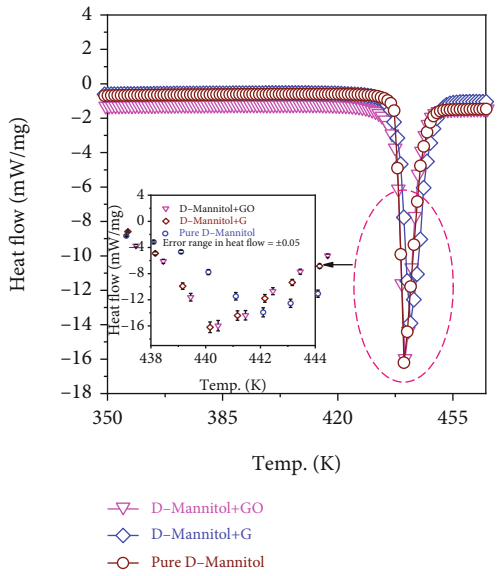

Figure 5: DSC thermograms of PDM, G/PDM, and GO/PDM powder samples.

generation; however, the measurement is done under steady-state condition where PDM, G/PDM, and GO/PDM undergo a phase transition at 433 K, 432.5 K, and 430 K. As hot-side temperature increases, the V_{OC} of the TEG also increases.

When hot-side temperature is 330 K with the cold-side temperature of 301 K, the open circuit voltages (V_{OC}) thus obtained in PDM, G/PDM, and GO/PDM are 0.35 V, 0.7 V, and 0.9 V, respectively. The V_{OC} of TEG attached with PDM, G/PDM, and GO/PDM increases with increase in hot-side temperature. Due to external heat, the PDM in the hot side of TEG starts melting at 433 K so there is a gradual increase in voltage. When the hot-side temperature reaches 436.85 K, voltage produced is also at maximum and it remains constant for 10 minutes till hot-side temperature reaches 440 K. At this stabilized temperature, the maximum voltage thus obtained with is 1.23 V from TEG with PDM at $\Delta T \backsim 118$ K.

When G/PDM is used, melting starts at 432.5 K and reaches a peak temperature at 442.25 K. The V_{OC} of G/PDM attached TEG is notably high when compared to bare PDM attached TEG in the measured hot-side temperature. Due to high thermal conductivity of graphite, it enhances the heat transfer rate of PCM and increases the hot-side temperature of TEG, which results in the maximum open circuit voltage 2.5 V at $\Delta T \backsim 118$ K.

When GO/PDM is used, melting starts at 430 K due to improved thermal conductivity and reaches a peak temperature at 440.4 K. Voltage thus produced is 4.5 V at $\Delta T \backsim 118$ K which is relatively high as compared to PDM and G.

Figure 6(c) shows the open circuit voltage with respect to time. When heater is off at 448 K, PCM stops melting and it starts releasing the stored heat. At this junction, the temperature difference is maintained for actual duration between hot and cold side of TEG. The maximum voltage drawn during the process of heater-off condition from the TEG with only PDM, G/PDM, and GO/PDM is 0.809 V, 2 V, and 2.9 V at $\Delta T \backsim 95$ K. The maximum time duration for voltage generation during the process of heater-off condition with only PDM, G/PDM, and GO/PDM is 25, 30, and 40 minutes, respectively.

3.5. Closed Circuit Voltage of TEG. The measured V_L during heater on and off is shown in Figures 7(a) and 7(b), and the measured I_L during heater on and off is shown in Figures 8(a) and 8(b). When heater is on, the hot-side temperature is 330 K and cold-side temperature is 301 K and the V_L obtained for only PDM, G/PDM, and GO/PDM is 0.1 V, 0.25 V, and 0.5 V. Due to increase in heat, the PDM starts melting, and

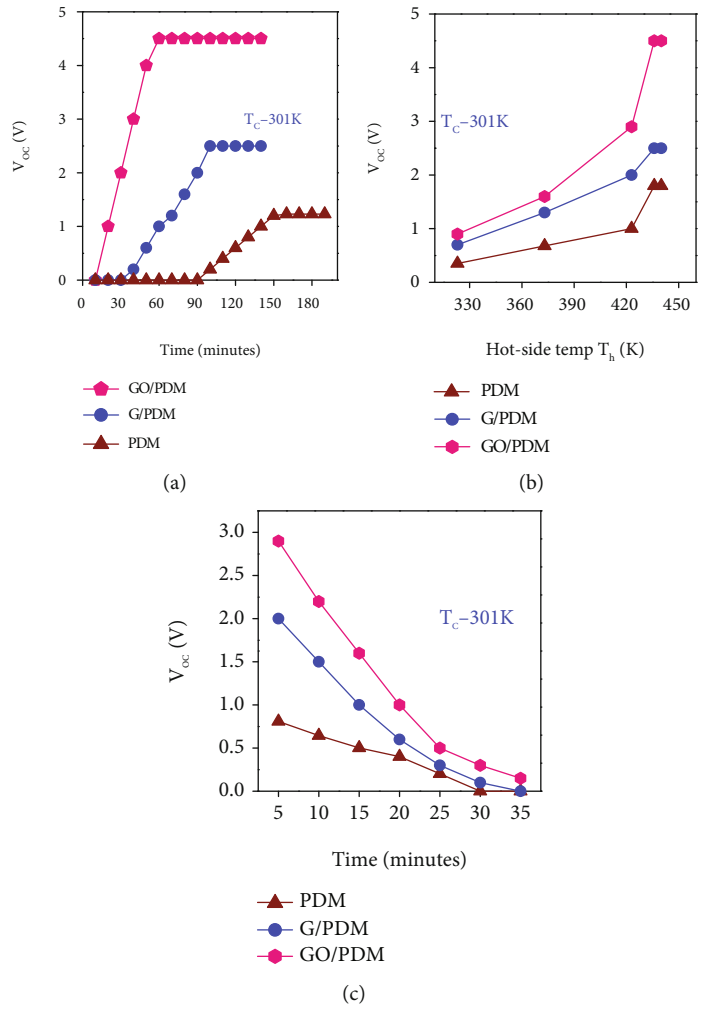

Figure 6: (a) Open circuit voltage (V_{OC}) vs. time (min) for only PDM, G/PDM, and GO/PDM. (b) Open circuit voltage (V_{OC}) vs. hot-side temperature (T_h) during heater on. (c) Open circuit voltage (V_{OC}) vs. time (min) during heater off.

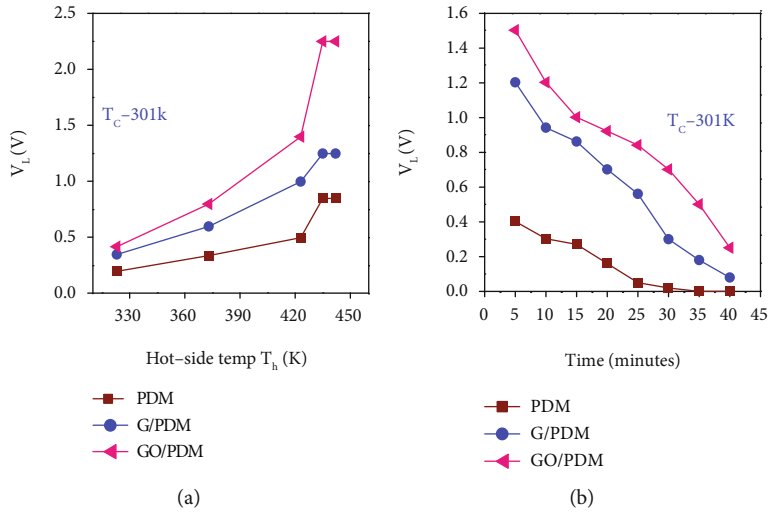

Figure 7: (a) Closed circuit voltage (V_L) vs. hot-side temperature (T_h) during heater on. (b) Closed circuit voltage (V_L) vs. time (min) during heater off.

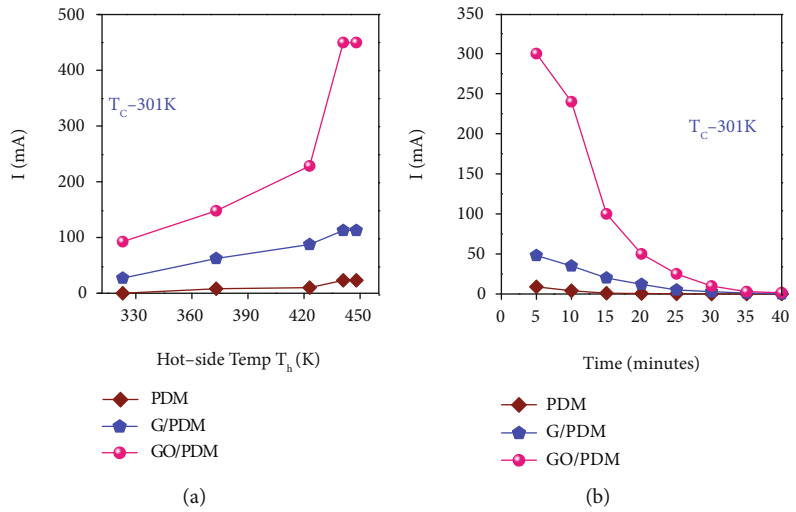

Figure 8: (a) Load current (I_L) vs. hot-side temperature (T_h) during heater on. (b) Load current (I_L) vs. time (min) during heater off.

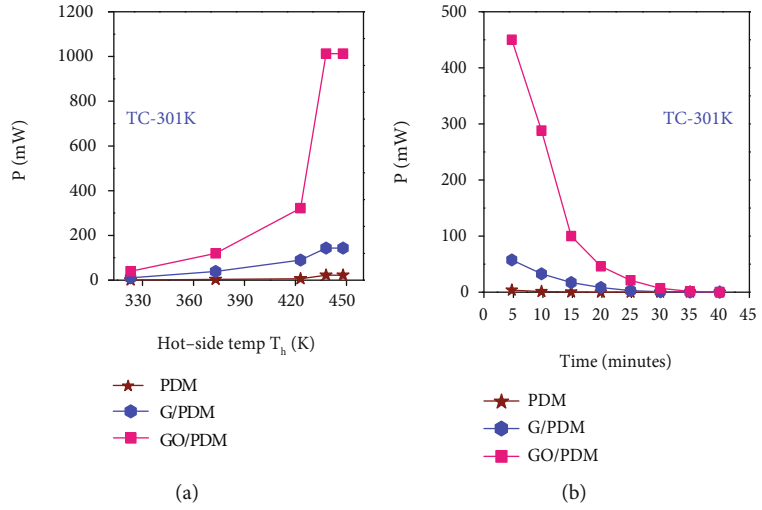

Figure 9: (a) Output power (P) vs. hot-side temperature (T_h) during heater on. (b) Output power (P) vs. time (min) during heater off.

the closed circuit voltage is relatively low compared to open circuit voltage due to drop across current and internal resistance. The maximum voltages thus obtained for only PDM, G/PDM, and GO/PDM are 0.8 V, 1.25 V, and 2.25 V, respectively, for $\Delta T \backsim 118$ K. And the stabilized maximum value of current is 26 mA, 115 mA, and 450 mA, respectively, for $\Delta T \backsim 118$ K. Further, when PDM is kept in the hot side of TEG, the effect of heat fluctuations can be reduced and the constant heat can also be maintained, which assists to protect the TEG. Interestingly, at heater-off condition, the maximum voltages generated for time duration with only PDM, G-PDM, and GO-PDM are 0.402 V, 1.2 V, and 1.5 V with 25, 30, and 40 minutes, respectively, for $\Delta T \backsim 95$ K.

3.6. Power Output of TEG. Power output thus obtained during closed circuit condition during heater on and off is shown in Figures 9(a) and 9(b). During heater-on condition, when hot-side temperature is 330 K and cold-side temperature is 301 K, the output power obtained using only PDM, G-PDM, and GO-PDM is 0.9 mW, 5.25 mW, and 12.5 mW. As T_h increases, generated power from TEG also increases in PDM, G-PDM, and GO-PDM to 22.1 mW, 143 mW, and 1012.5 mW at $\Delta T \backsim 118$ K. During heater-off condition, the maximum value of power generation by GO-PDM is 450 mW for 5 minutes, whereas it decreases gradually to 30 mW after 25 minutes. The maximum output power of TEG during heater-off condition with only PDM, G-PDM, and GO-PDM is 15 mW, 70 mW, and 450 mW for the maximum time duration of 20, 30, and 40 minutes.

4. Conclusion

We have effectively demonstrated the enhancement in the power output of commercially available TEG by attaching graphite (G) and graphene oxide (GO) decorated D-mannitol nanocomposites. Presence of G and GO in the matrix of D-mannitol has been confirmed by XRD and FE-SEM. Using GO/PDM, thermal conductivity was improved compared to

G/PDM. The open circuit voltage and short circuit current of TEG attached in the PDM, G/PDM, and GO/PDM were recorded for heating and cooling in the temperature of 325-450 K. Particularly, the maximum open circuit voltage of PDM, G/PDM, and GO/PDM drawn is 1.23 V, 2.5 V, and 4.5 V at $\Delta T \backsim 118$ K. Further, the maximum power generation of PDM, G/PDM, and GO/PDM during heater-on condition is 22.1 mW, 143 mW, and 1012.5 mW at $\Delta T \backsim 118$ K. During heater-off condition using stored heat, the maximum power generated by PDM, G/PDM, and GO/PDM was 3.618 mW, 57.6 mW, 450 mW and at $\Delta T \backsim 95$ K. Thus, the present study indicates addition of graphene oxide with D-mannitol PCM could be a potential phase-change material for transient heat recovery.

Data Availability

The data that support the findings of this study are available from the corresponding author on request.

Conflicts of Interest

The authors declare that they have no conflicts of interest.

Authors' Contributions

The contribution of the work is as follows: (1) design and conceptualization of the work were done by SP and JRK; (2) synthesis and experiment were performed by LJ and MM; (3) analysis and discussion were done by LJ, SP, MM, and JRK; (4) manuscript was written by LJ, JRK, and SP.

Acknowledgments

We acknowledge SRM (SCIF) for providing research facility.

References

[1] W. He, G. Zhang, X. Zhang, J. Ji, G. Li, and X. Zhao, "Recent development and application of thermoelectric generator and cooler," *Applied Energy*, vol. 143, pp. 1–25, 2015.

[2] K. Biswas, J. He, I. D. Blum et al., "High-performance bulk thermoelectrics with all-scale hierarchical architectures," *Nature*, vol. 489, no. 7416, pp. 414–418, 2012.

[3] H. Liu, X. Shi, F. Xu et al., "Copper ion liquid-like thermoelectrics," *Nature Materials*, vol. 11, no. 5, pp. 422–425, 2012.

[4] S. Perumal, M. Samanta, T. Ghosh et al., "Realization of high thermoelectric figure of merit in GeTe by complementary Co-doping of Bi and In," *Joule*, vol. 3, no. 10, pp. 2565–2580, 2019.

[5] L. D. Zhao, S. H. Lo, Y. Zhang et al., "Ultralow thermal conductivity and high thermoelectric figure of merit in SnSe crystals," *Nature*, vol. 508, no. 7496, pp. 373–377, 2014.

[6] L. Jame, "A Comprehensive Review on Thermoelectric Generator for Energy Harvesting," *Advances in Automation, Signal Processing, Instrumentation, and Control*, vol. 700, no. 1897, 2021.

[7] Y. Zhang, M. Cleary, X. Wang et al., "High-temperature and high-power-density nanostructured thermoelectric generator for automotive waste heat recovery," *Energy Conversion and Management*, vol. 105, pp. 946–950, 2015.

[8] N. Muralidhar, M. Himabindu, and R. V. Ravikrishna, "Modeling of a hybrid electric heavy duty vehicle to assess energy recovery using a thermoelectric generator," *The Energy Journal*, vol. 148, pp. 1046–1059, 2018.

[9] L. D. Zhao, V. P. Dravid, and M. Kanatzidis, "The panoscopic approach to high performance thermoelectrics," *Environmental Sciences*, vol. 7, no. 1, pp. 251–268, 2014.

[10] J. Yagi and T. Akiyama, "Storage of thermal energy for effective use of waste heat from industries," *Journal of Materials Processing Technology*, vol. 48, no. 1-4, pp. 793–804, 1995.

[11] T. Oya, T. Nomura, N. Okinaka, and T. Akiyama, "Phase change composite based on porous nickel and erythritol," *Applied Thermal Engineering*, vol. 40, pp. 373–377, 2012.

[12] N. Sarier and E. Onder, "Organic phase change materials and their textile applications: an overview," *Thermochimica Acta*, vol. 540, pp. 7–60, 2012.

[13] S. Mondal, "Phase change materials for smart textiles – an overview," *Applied Thermal Engineering*, vol. 28, no. 11-12, pp. 1536–1550, 2008.

[14] R. Kandasamy, X. Q. Wang, and A. S. Appl, "Transient cooling of electronics using phase change material (PCM)-based heat sinks," *Thermal Engineering*, vol. 28, no. 8-9, pp. 1047–1057, 2008.

[15] M. Augspurger, K. K. Choi, and H. S. Udaykumar, "Optimizing fin design for a PCM-based thermal storage device using dynamic Kriging," *International Journal of Heat and Mass Transfer*, vol. 121, pp. 290–308, 2018.

[16] X. Wang, Y. Guo, J. Su, X. Zhang, N. Han, and X. Wang, "Microstructure and thermal reliability of microcapsules containing phase change material with self-assembled graphene/organic nano-hybrid shells," *Journal of Nanomaterials*, vol. 8, no. 6, 2018.

[17] Y. Li, J. Li, Y. Deng, W. Guan, X. Wang, and T. Qian, "Preparation of paraffin/porous TiO_2 foams with enhanced thermal conductivity as PCM, by covering the TiO_2 surface with a carbon layer," *Applied Energy*, vol. 171, pp. 37–45, 2016.

[18] W. Wang, V. Cionca, N. Wang, M. Hayes, B. O'Flynn, and C. O'Mathuna, "Thermoelectric Energy Harvesting for Building Energy Management Wireless Sensor Networks," *International Journal of Distributed Sensor Networks*, vol. 9, no. 6, 2013.

[19] M. Guan, K. Wang, D. Xu, and W.-H. Liao, "Design and experimental investigation of a low-voltage thermoelectric energy harvesting system for wireless sensor nodes," *Energy Conversion and Management*, vol. 138, pp. 30–37, 2017.

[20] M. Jaworski, M. Bednarczyk, and M. Czachor, "Experimental Investigation of Thermoelectric generator with PCM module," *Applied Thermal Engineering*, vol. 110, p. 163, 2013.

[21] S. A. Atouei, A. A. Ranjbar, and A. Rezania, "Experimental investigation of two-stage thermoelectric generator system integrated with phase change materials," *Appl. Energy*, vol. 208, no. 332, pp. 332–343, 2017.

[22] X. F. Zheng, C. X. Liu, R. Boukhanouf, Y. Y. Yan, and W. Z. Li, "Experimental study of a domestic thermoelectric cogeneration system," *Applied Thermal Engineering*, vol. 62, no. 1, pp. 69–79, 2014.

[23] L.-W. Fan, X. Fang, X. Wang et al., "Effects of various carbon nanofillers on the thermal conductivity and energy storage properties of paraffin-based nanocomposite phase change materials," *Applied Energy*, vol. 110, no. 163, pp. 163–172, 2013.

[24] T.-P. Teng, B.-G. Lin, and Y.-Y. Yeh, "Characterization of heat storage by nanocomposite-enhanced phase change materials," *Advances in Materials Research*, vol. 287-290, pp. 1448–1455, 2011.

[25] S. Manikandan, C. Selvam, N. Poddar, K. Pranjyal, R. Lamba, and S. C. Kaushik, "Thermal management of low concentrated photovoltaic module with phase change material," *Journal of Cleaner Production*, vol. 219, pp. 359–367, 2019.

[26] L. Jame, J. R. Kumar, S. Perumal, Y. Jeyashree, and M. Moorthy, "Experimental investigation of thermoelectric power generator using D-mannitol phase change material for transient heat recovery," *ECS Journal of Solid State Science and Technology*, vol. 10, no. 6, article 061005, 2021.

[27] Y. Jia, "Analysis of Nonlinear Transient Energy Effect on Thermoelectric Energy Storage Structure," *Maternité*, vol. 13, no. 16, p. 3639, 2020.

[28] M. I. Kumar, S. S. Shyam, E. J. Kirupavathy, S. Sureshkumar, and M. Vinolia, "Synthesis and characterization of novel reduced graphene oxide supported barium niobate (RGOBN) nanocomposite with enhanced ferroelectric properties and thermal stability," *Journal of Materials Science: Materials in Electronics*, vol. 29, no. 22, pp. 19228–19237, 2018.